



Integrated Dynamics and Controls Modeling for the Space Interferometry Mission (SIM)

David W. Miller, Olivier L. de Weck, Scott A. Uebelhart
Space Systems Laboratory, Massachusetts Institute of Technology
77, Massachusetts Avenue, Cambridge, MA 02139
Phone (617) 253-3288, millerd@mit.edu or deweck@mit.edu

Robert Grogan, Ipek Basdogan
Jet Propulsion Laboratory, California Institute of Technology
4800 Oak Grove Drive, Pasadena, CA 91109

Session 6.09: Interferometric Systems and Remote Sensing

Integrated Dynamics and Controls Modeling for the Space Interferometry Mission (SIM)^{1,2}

David W. Miller, Olivier L. de Weck, Scott A. Uebelhart
Space Systems Laboratory, Massachusetts Institute of Technology
77, Massachusetts Avenue, Cambridge, MA 02139
Phone (617) 253-3288, millerd@mit.edu or deweck@mit.edu

Robert Grogan, Ipek Basdogan
Jet Propulsion Laboratory, California Institute of Technology
4800 Oak Grove Drive, Pasadena, CA 91109

Abstract—Integrated dynamics and controls modeling provides confidence in the design of complex opto-mechanical space systems before integration and launch. This paper discusses the underlying process for modeling and analysis based on linear time-invariant systems theory in the frequency domain. Results are presented for the Space Interferometry Mission. Performance predictions are made for phasing as represented by optical pathlength difference (OPD) metrics and pointing given by wavefront tilt (WFT) metrics for one science and two guide star interferometers. The disturbance source is reaction wheel induced jitter caused by flywheel and bearing imperfections. Results are obtained for a broadband and a narrowband disturbance analysis, critical modes and wheel speed determination, modal sensitivity analysis and isoperformance analysis. The findings suggest that the critical frequency region for SIM is in the range from 160-190 Hz with both optics and attitude control loops closed. It appears that a reduction in wheel disturbance by 30% would have a similar effect than an increase in optical control bandwidth from 100 to 180 Hz.

TABLE OF CONTENTS

1. INTRODUCTION
2. MODEL CONDITIONING AND ASSEMBLY
3. RWA DISTURBANCE ANALYSIS
4. CRITICAL WHEEL SPEEDS AND MODES
5. SENSITIVITY AND ISOPERFORMANCE
6. CONCLUSIONS AND RECOMMENDATIONS
- A. DOCS FRAMEWORK DESCRIPTION

1. INTRODUCTION

Background

The accurate prediction of the dynamic opto-mechanical performance of complex interferometric spacecraft prior to launch is essential before committing substantial resources towards a particular system architecture. Additionally, it is desirable to determine which modal or physical system parameters are dynamic performance drivers. The Space

Interferometry Mission (SIM) will attempt to achieve a 4 μ arcsecond astrometric precision for 20th magnitude stars during a 5-year mission life [1],[2]. In order to achieve this precision, SIM (see Figure 1) features one science and two guide star interferometers. A fourth interferometer (spare) is not analyzed in this paper. A more detailed description of the SIM optical system and fringe acquisition and tracking process is contained in reference [3].



Figure 1 Space Interferometry Mission (SIM) concept

The processes of fringe acquisition and fringe tracking require stabilization of the starlight and internal metrology pathlength to a fraction of the wavelength λ of light. The performance requirements can be subdivided into phasing and pointing metrics as shown in Table 1.

Table 1 SIM opto-mechanical performance requirements

performance z_i	i	units	requirement
Starlight OPD #1-3	1,2,3	nm	10 (RMS)
Internal Metrology OPD #1-3	4,5,6	nm	20 (RMS)
Starlight WFT #1-3	7,8,9	asec	0.210 (RSS)

Note: #1-3 refers to the one science and two guide star interferometers.

¹ 0-7803-6599-2/01/\$10.00 © 2001 IEEE

² Updated December 12, 2000

The symbol z is used to designate performance metrics. The starlight OPD comprises the difference in starlight pathlength from an incoming planar stellar wave front through two arms of an interferometer to the fringe detector. The internal metrology OPD comprises the internal pathlength difference out to the optical fiducials attached to the siderostat mirrors [3]. Note that RMS refers to the root-mean-square of the optical pathlength difference according to

$$\sigma_{z,i} = E \left[OPD(t)_i^2 \right]^{1/2} \quad (1.1)$$

where $OPD(t)_i$ refers to the OPD of the i -th interferometer and $E[]$ is the expectation operator. The RSS pointing metrics are obtained by computing the root-sum-square of wave front tilt in the X and Y-axes for arms 1 and 2 of each interferometer:

$$\sigma_{z,j} = \left[\sigma_{WFT X,1}^2 + \sigma_{WFT Y,1}^2 + \sigma_{WFT X,2}^2 + \sigma_{WFT Y,2}^2 \right]^{1/2} \quad (1.2)$$

These are 1σ requirements broadband (integrated over all frequencies). These requirements have to be met in the presence of random (stochastic) mechanical and electronic disturbances. It is expected that the reaction wheel assembly (RWA) - used for attitude control - will be the largest disturbance source.

It was decided to subject the mission concept to multidisciplinary modeling and simulation to verify the soundness of the approach and to identify critical system parameters that are likely to be performance drivers. The analysis presented here is a complementary analysis to the JPL internal efforts presented earlier by Basdogan, Grogan et al [3]. The model that was used for this study is the open loop SIM Classic integrated nanodynamics model (see Figure 2) developed by the Jet Propulsion Laboratory (JPL). The original model has 103 outputs and 20 inputs, is in 2nd order modal form and contains no disturbance and controller states [3]. In this study we only consider 6 inputs (RWA) and 34 outputs, which are combined, among others, into the 9 performance metrics shown in Table 1. Performance metrics not discussed in this paper are: Front End Camera (FEC) wavefront tilt, ACS angle pointing requirements and external metrology pathlength. The 6 disturbance inputs w are as follows:

1-3: RWA Forces [F_x F_y F_z]

4-6: RWA Torques [M_x M_y M_z]

Note that the RWA is not the only expected disturbance source and that only a fraction of the allowable errors in Table 1 can be caused by it. Other likely sources include attitude determination noise and other mechanical actuators. The allocation of total allowable errors due to all expected disturbance sources is subject to the error budgeting process.

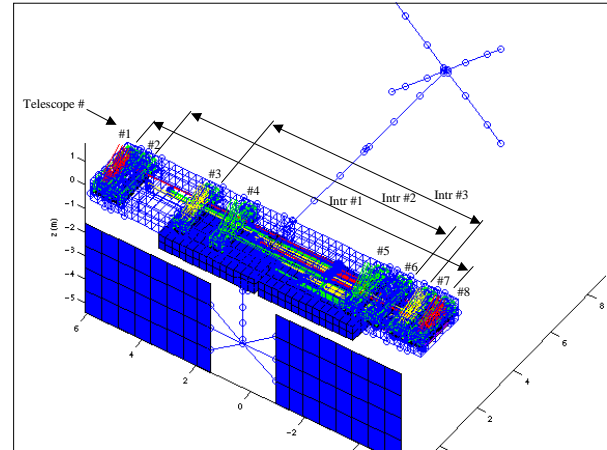


Figure 2 SIM Integrated Nanodynamics Model (JPL)

Problem Formulation

For the SIM integrated nanodynamics model compute the predicted performance RMS and RSS values for realistic broadband and narrowband RWA disturbances and compare the results. The disturbance processes are assumed to be random, stationary and steady state. Estimate the modal frequency and damping sensitivity of the performances and predict the critical modes and frequency bands that will drive the dynamic performance for SIM. Trade two key physical or modal parameters of the system with respect to each other such that the desired performance is maintained (isoperformance).

Methodology

Figure 3 summarizes the methodology that was followed in order to solve the problem formulated above. It also serves as an outline to this paper. The first step consists of assembling and conditioning the integrated model, which is based on the open-loop opto-mechanical plant shown in Figure 2. This also includes a description of the broadband and narrowband RWA disturbance models (Section 2). A broadband and narrowband RWA disturbance analysis is conducted and the results are compared (Section 3). Based on the disturbance analysis results, we attempt to identify critical wheel speeds, frequency regions and modal parameters of SIM (Section 4). A sensitivity analysis for these critical modal parameters reveals how sensitive the performance metrics are to individual modal parameters such as frequency, damping and modal mass. An isoperformance analysis allows trading key parameters with respect to each other, while constraining the system performance to the desired levels (Section 5). Finally Section 6 summarizes the paper, draws conclusions and makes recommendations for future research. The software tools developed in the context of this research are part of the DOCS (Dynamics-Optics-Controls-Structures) toolset and are briefly described in the Appendix.

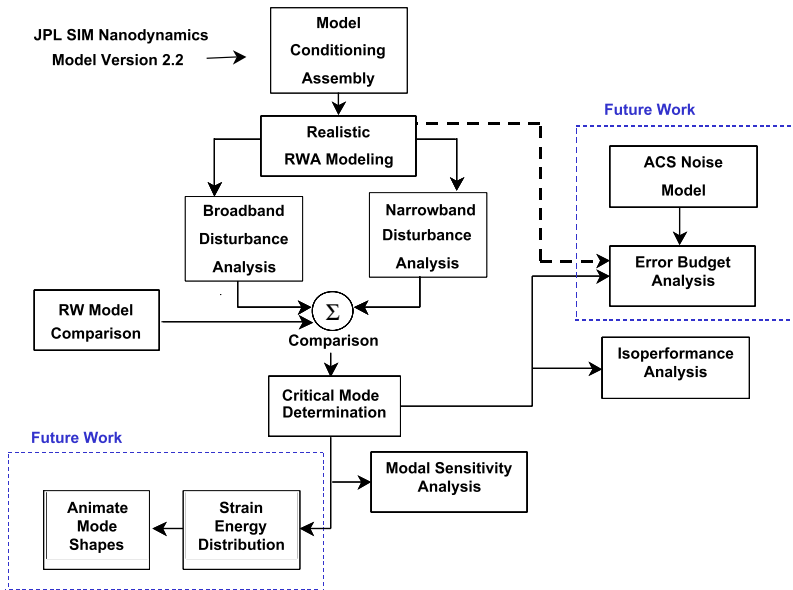


Figure 3 Paper outline and methodology

2. MODEL CONDITIONING AND ASSEMBLY

Model assembly is the process of appending the structural, optical, controls and disturbance sub-models into an overall dynamics model. Model conditioning and reduction are important steps for two reasons. First the numerical conditioning of the unconditioned, assembled model is generally poor since it contains unobservable and/or uncontrollable states. Secondly reducing the model from initially over 2200 states to a few hundred (important) states allows significant CPU timesavings in the disturbance and sensitivity analysis.

Model Conditioning

First a channel reduction is performed, which only retains the input-output channels of interest. Then the 3 translational rigid body modes are removed from the model, since they are not observable in any of the performance metrics of interest. The remaining system dynamics are contained in the state space system

$$\begin{aligned} \dot{q}_p &= A_p q_p + B_{pu} u + B_{pw} w \\ y &= C_p q_p + D_{pu} u + D_{pw} w \end{aligned} \quad (2.1)$$

Here A_p is the plant state transition matrix, B_{pu} and B_{pw} are the control input and disturbance input matrices, C_p is the plant output matrix and D_{pu} and D_{pw} are the control and disturbance feed through matrices, respectively. The output vector y is used to define the optical performance metrics of Table 1. This system contains 2148 states and is poorly conditioned, since not all states are observable or

controllable. Additionally the system (2.1) is only neutrally stable, since the uncontrolled rotational rigid body modes give rise to poles at the origin of the s-plane.

Balancing Method

Previous efforts at balancing large order systems such as SIM were unsuccessful using the traditional MATLAB routines such as `balreal.m` based on research by Moore [4] and Laub [5]. This is largely caused by the ill-conditioned inversion of very small singular values. The model balancing routine used here goes through several steps described by Mallory [6] and Uebelhart [11], including a pre-balancing step, and

results in a balanced truncated model of smaller order than the original. The balanced truncation removes slightly controllable and slightly observable states as the system is balanced to maintain good numerical conditioning. The remaining system has 1960 states (see Figure 4).

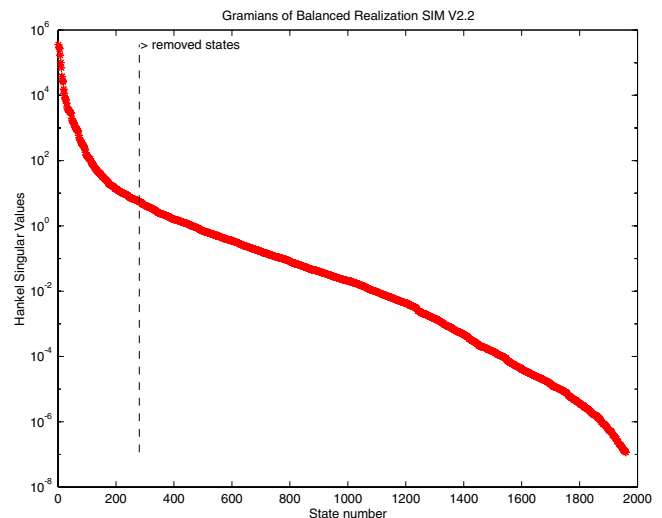


Figure 4: Gramian values for balanced truncated state space model of SIM Classic (version 2.2)

Model Reduction

The Gramian values (diagonal of Gramian matrix) shown by the very low values on the right side of Figure 4 correspond to modes of low controllability/observability and can be removed from the model without significantly affecting the retained dynamics. The following inequality can be used to bound the relative error on the RMS of the outputs y as a function of the Hankel singular values σ^H of the balanced reduced system:

$$\frac{\Delta\sigma_y}{\bar{\sigma}_y} < \frac{1}{2} \frac{\sum_{i=k+1}^n \sigma_i^H}{\sum_{i=1}^k \sigma_i^H} \quad (2.2)$$

The allowable error on the RMS of the plant outputs y was set to 0.01%. By evaluating the inequality (2.2) recursively we retain the first 316 states corresponding to the largest singular values. This reduced model is subsequently used for the narrowband RWA disturbance analysis. The broadband analysis uses a larger model with 1063 states, since it is computationally less expensive. Figure 5 shows a comparison of the transfer functions from input 1 (RWA Fx) to output 1 (Star OPD #1) for the original unconditioned model (2148 states), the moderately reduced model used for the broadband analysis (1063 states) and the aggressively reduced model (316 states) used for the narrowband disturbance analysis.

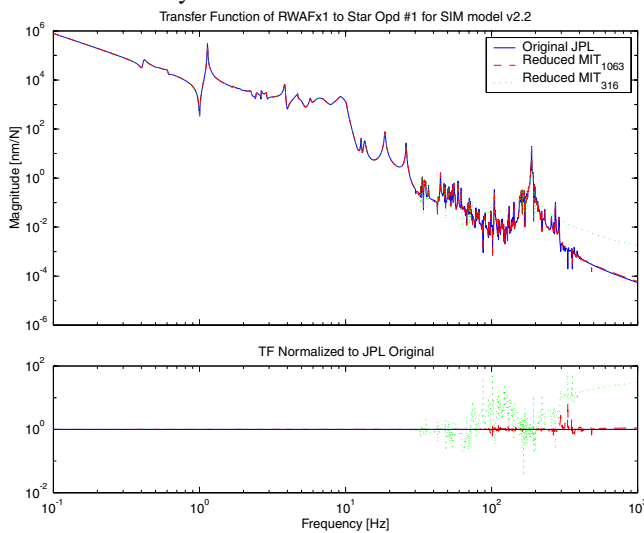


Figure 5 Transfer function comparison for conditioned models from RWA Fx to Star OPD #1 (open loop)

The upper subplot shows a magnitude comparison and the transfer functions overlay well up to roughly 200 Hz. A quantification of the deviation of the reduced models from the original transfer function is given in the lower subplot. Because the narrowband analysis requires many iterations of the disturbance analysis (one at each wheel speed), a smaller model was used for that purpose (316 states). A deviation of the slope of the transfer function backbone is observed above 200 Hz for this reduced model.

Model Assembly

Next an ACS model in state space form is appended in order to stabilize the rotational rigid body modes. The controller is designed with 3 parallel proportional-derivative (PD) channels with a second order low-pass filter (LPF). The controller for a single channel is given as

$$K_a(s) = \frac{[K_r s + K_p] \omega_i^2}{s^2 + 2\zeta_i \omega_i s + \omega_i^2} \quad (2.3)$$

Here K_r and K_p are the rate and proportional gain and ω_i and ζ_i are the rolloff filter frequency and damping, respectively. The purpose of the ACS controller is merely to stabilize the rigid body modes of the system, such that subsequent analyses can be conducted. The solution of Lyapunov equations for example requires that the system is stable and that the rigid body modes are controlled [7]. The gains are set such that the crossover frequency occurs at 10% of the frequency of the first flexible mode in the system. This results in an effective ACS bandwidth of 0.04 Hz (see Figure 6). The ACS reads in the three attitude angles, which would be provided by a star tracker. Sensor noise can be added to the model in the future. The subsequent analyses in section 3 assume that the attitude angle measurements are noise free.

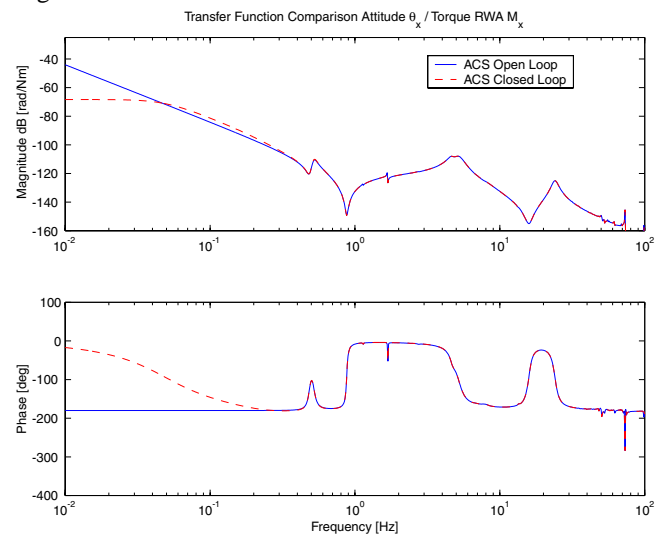


Figure 6 Transfer function (ACS) from RWA Mx to θ_x

The effect of closing the optics loops (for example between internal metrology and the optical delay lines) is captured by filtering the controlled optics metrics with a high-pass filter.

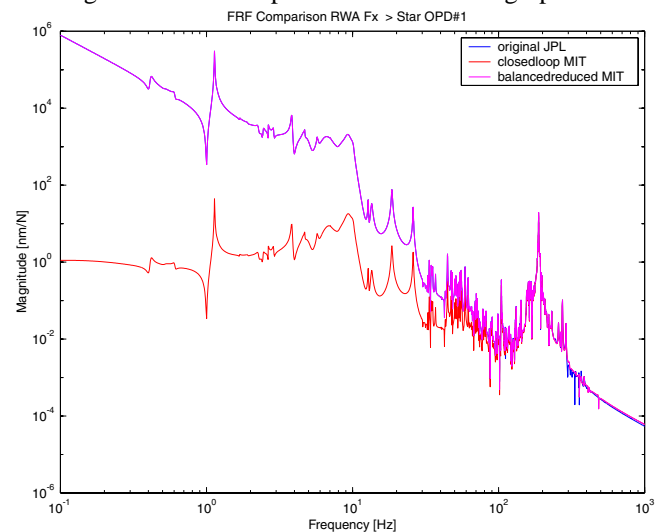


Figure 7 Effect of closing optics loops (100 Hz bandwidth).

The filter equation is:

$$K_o(s) = \frac{s^2}{s^2 + 2\zeta_o\omega_o s + \omega_o^2} \quad (2.4)$$

Here ω_o and ζ_o are the optical control bandwidth [rad/sec] and damping ratio (set to 0.707), respectively. The disadvantage of this approach is that stability robustness considerations are not taken into account. The effect of closing optics loops can be seen in Figure 7. Note that the filter corner frequency ω_o is set to the expected optical control bandwidth for SIM (100 Hz). This quantity will be traded later in the isoperformance analysis. Disturbances are attenuated below this frequency as seen by the red curve in the transfer function of Figure 7. The blue and magenta curves represent the original JPL and the balanced/reduced MIT models, respectively. Once all the disturbance, plant and controller dynamics are available they are appended into an overall system as shown in Figure 8. Note that the RWA noise is considered to be process noise, whereas the attitude determination noise is sensor noise in the ACS loop (neglected in this analysis).

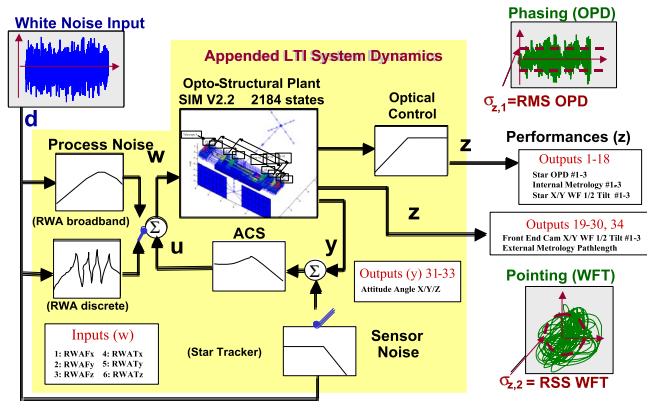


Figure 8 Block Diagram of assembled SIM Model

Verifying that none of the poles of the closed loop system lie in the right half-plane (RHP) ensures absolute stability of the closed loop system.

3. RWA DISTURBANCE ANALYSIS

The stochastic disturbances introduced by spinning reaction wheels are due to static and dynamic imbalances of the flywheels, bearing chatter and other mechanical imperfections. A comprehensive review of the theory of reaction wheel disturbance modeling is given by Masterson [8]. The most important stochastic variable is the wheel speed. Assuming that the wheel speeds are allowed to vary with uniform probability density between 10-66 RPS (expected operating range) leads to the broadband RWA disturbance analysis presented in the next subsection.

RWA Broadband Disturbance Model

This disturbance model takes frequency and magnitude content from laboratory wheel tests and computes

broadband PSD's for a specific RWA [8]. In this case we assumed three (3) Hubble Space Telescope (HST)-type reaction wheels [9] in a 90-degree triad configuration. We assume that the wheel speed is given by a uniform probability density function over the range 10 to 66 RPS.

Once the PSD's for the RWA disturbance are obtained a non-linear constrained optimization is performed in order to obtain a matching state space-shaping filter for each RWA disturbance channel. This is necessary in order to append the disturbance dynamics into the state space formulation for subsequent Lyapunov and sensitivity analysis [7]. The matching is achieved by constraining the first non-zero PSD point to match the pre-whitening filter and by iterating on the objective function. The objective function is the difference between the cumulative RMS of the actual (data) PSD and the state space filter. The three parameters that are being optimized are the gain K_{rwa} , the lower corner ω_{lc} and the upper corner ω_{hc} in the following pre-whitening filter equation:

$$G_{RWA}(s) = \frac{K_{RWA}s^2}{(s + w_{lc})^2 (s + w_{hc})^4} \quad (3.1)$$

The gain K_{rwa} will be traded against optical control bandwidth ω_o in the isoperformance analysis (Section 5). The state space system that results shapes unit-intensity white noise to represent the "on average" RWA disturbance as shown in Figure 9 (for RWA disturbance component Fx).

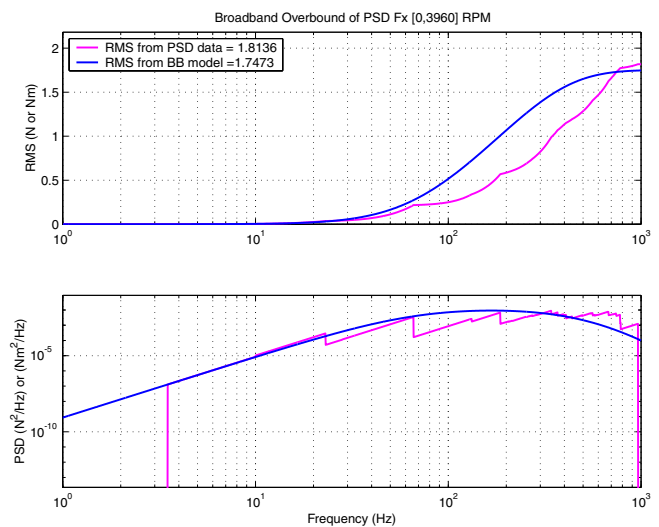


Figure 9: Broadband reaction wheel disturbance model (RWA Fx) for Hubble-type RWA with 3 wheels

Broadband Analysis Results

The following two figures show the results for the broadband disturbance analysis using the HST broadband disturbance model. The performance metrics considered are

Star OPD #1-3 (RMS). The first figure contains the results without optical control (only ACS is active).

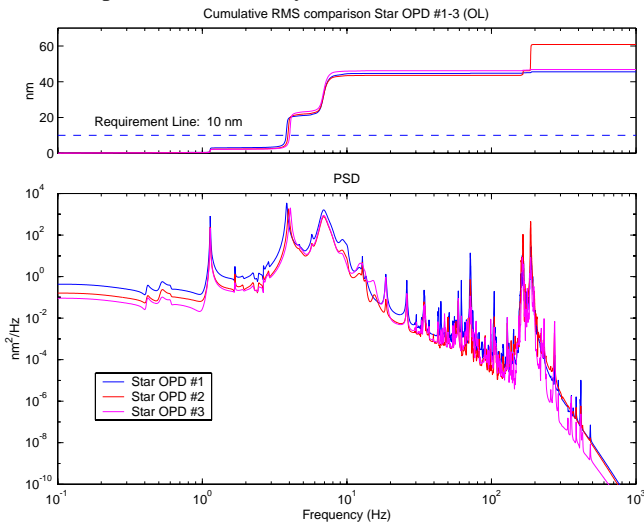


Figure 10: SIM broadband analysis assuming HST wheels for Star OPD#1-3 with optics loops open

The above figure shows the resulting PSD's (bottom plot) and cumulative RMS curves (top plot) with optics loops open for all three interferometers. As expected phasing requirements (10 nm) are not met with open optics loops and the most significant error contributions – as judged by the steps in the cumulative RMS – occur in the 4, 8 and 180 Hz regions. Figure 11 shows the results with closed optics loops.

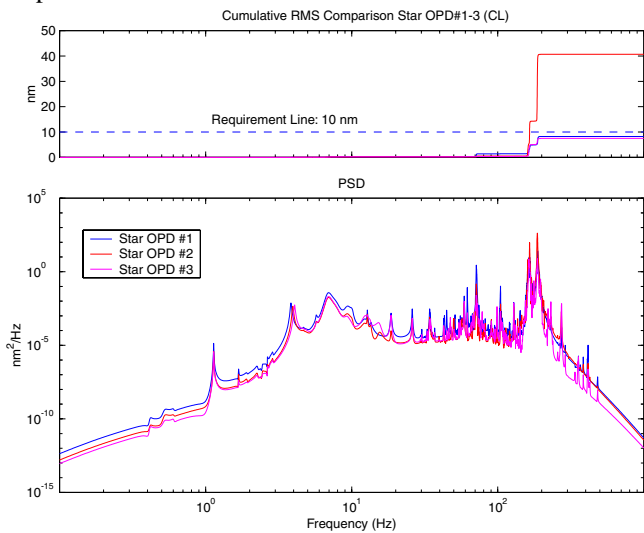


Figure 11 SIM broadband disturbance analysis assuming HST wheels for Star OPD#1-3 with closed optics

Analyzing these PSD's, we see that closing the optics loops reduces the magnitude of the PSD at the lower frequencies. The modes at ~180 Hz, however, are essentially unaffected, such that this frequency region remains as a significant source of OPD. Note that the required RMS of 10 nm is the total error allowed for SIM. The allowable error budgeted for the RWA contribution, however, is less than 10 nm (6 nm for the science fringe tracking budget). It is also

interesting to note that Star OPD #2 exceeds the 10 nm requirements line, whereas interferometers #1 and 3 remain within the requirement. The next two figures contain the results for Starlight WFT #1-3, corresponding to the pointing performance of the SIM interferometers.

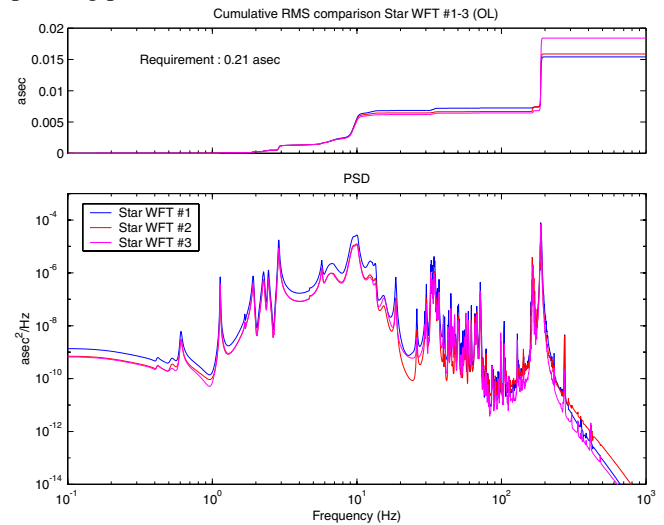


Figure 12: SIM broadband analysis using HST wheels for Star WFT#1-3 with optics loops open

We see that the pointing (WFT) error RMS has contributions around 7-10 Hz as well as in the 180 Hz region. We will attempt to quantify these contributions in Section 4 of this paper. It is interesting to note that the pointing requirements are satisfied by a good margin in the open loop (Figure 12) and closed loop case (Figure 13) for all interferometers. It is likely that the introduction of attitude determination noise will change these answers in the open loop case.

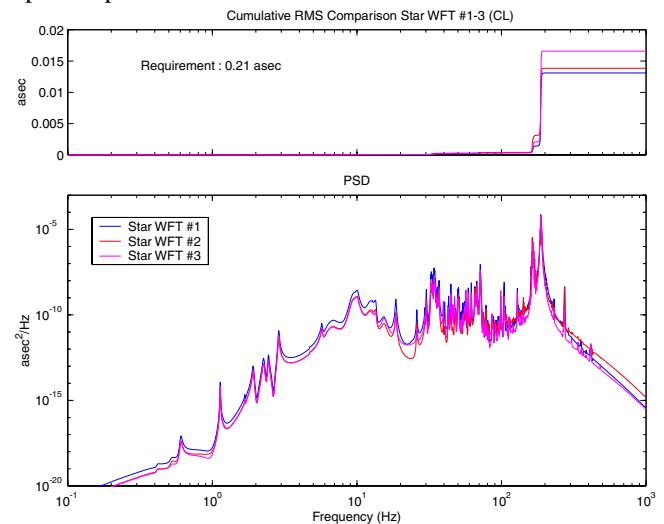


Figure 13 SIM broadband disturbance analysis (HST Wheels) for Star WFT#1-3 with closed optics loops

Narrowband Analysis Results

In the previous subsection the assumption was that the wheel speeds could vary from 10-66 RPS with uniform probability

density. Thus, averaged over long integration times during astrometric measurements, the RWA disturbance energy is “smeared” out in the frequency domain, even though the disturbances are tonal at any given instant in the time domain. In the narrowband disturbance analysis³, however, we assume that all three wheels are spinning at a constant speed. Thus “narrowband” in this instance refers to the assumption of stationary wheel speeds. Each wheel gives rise to a number of disturbance tones. For each wheel speed the RMS values of all performances are then computed. The wheel speed is then swept from 10 revolutions-per-second (RPS) to 66 RPS.

A state-space reaction wheel disturbance model was created assuming that each disturbance tone is a second-order system driven by white noise. This formulation is necessary for a subsequent sensitivity analysis, where the disturbance dynamics must be appended in the overall formulation. The (conservative) assumption is that all three wheels are spinning at the same speed. The 2nd order equation for each individual tone is

$$G_i(s) = \frac{k_i s}{s^2 + 2\zeta_i \omega_i s + \omega_i^2} \tag{3.2}$$

Here k_i , ω_i and ζ_i are the tonal gain, frequency and damping ratio respectively. The disturbance tones for the axial disturbance force (at 10 RPS) of a single reaction wheel are shown in Figure 14.

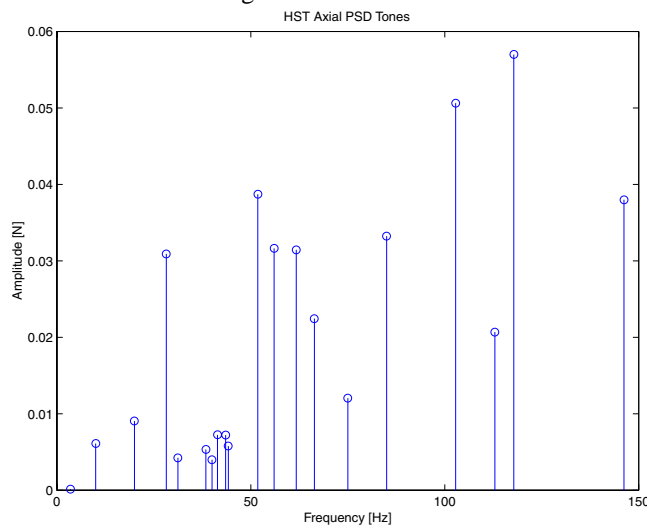


Figure 14: Wheel disturbance tones (axial 10 RPS)

The contributions from each wheel are summed to produce a narrowband (stationary wheel speed) reaction wheel assembly PSD. The state-space model is checked by determining that its power is equal to that of the tones. While the tones can be added up (and square rooted) to

³ We could also refer to this as a *tonal* analysis or a *discrete* analysis. This was avoided, however, in order to prevent confusion with a discrete time or z-domain analysis.

produce the cumulative RMS plot, there are two methods for the state-space system. A Lyapunov approach [7] can be used to find the RMS value, or the transfer function matrix of the system (with a properly dense frequency vector) can be computed to solve for the cumulative RMS value by integrating under the PSD. The square root of the integral under the PSD results is the RMS value.

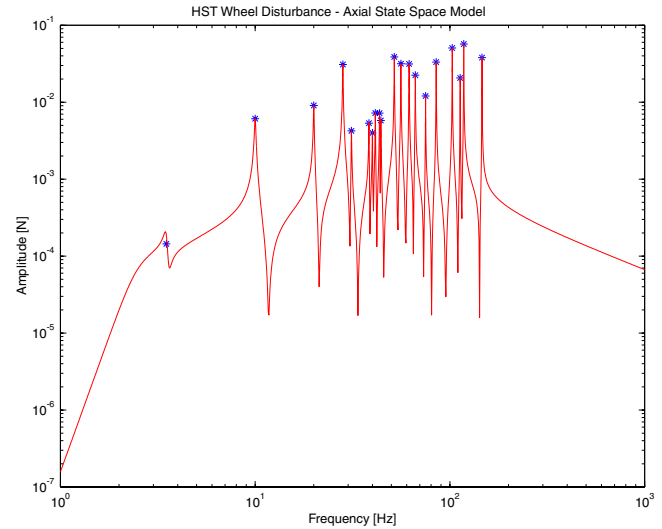


Figure 15 State space approximation of tonal RWA disturbance (component RWA Fz is shown)

Figure 15 shows the amplitude spectrum of the state space approximation (red continuous curve) and the individual tones (blue asterisk). The state space approximation matches the tonal RMS, and the energy is accumulated at the correct frequencies as shown in Figure 16.

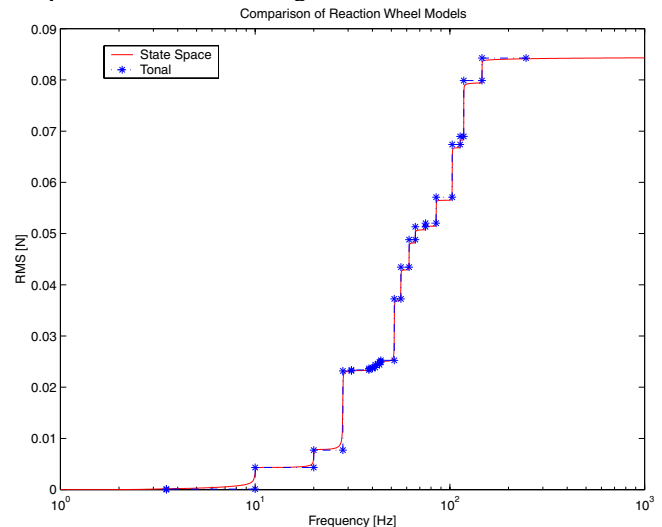


Figure 16 Cumulative RMS verification of narrowband RWA (state space) disturbance model

These next two figures (17 and 18) show representative examples for the narrowband disturbance analysis. They indicate the “worst-case” performances by scanning over all wheel speeds. The analysis is computed for the range from

10 RPS to 66 RPS, which is assumed to be the wheel operating range.

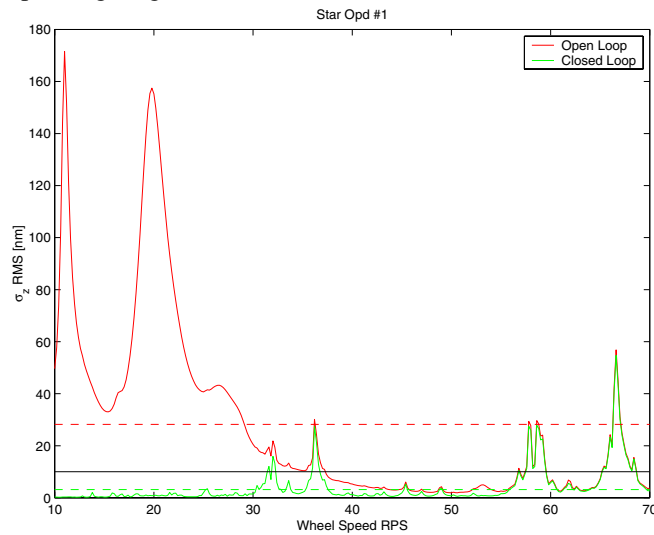


Figure 17 Narrowband disturbance analysis for Star OPD#1

We note that the open loop and closed loop results are similar above 30 RPS. Below this speed, the 0.35 sub-harmonic of the wheels is the driving source of disturbance. Since it acts at the frequency below the wheel speed (i.e. always below 66 Hz), it drives many of the modes below 10 Hz. These are attenuated with the optical control loops closed as shown in Figure 17. Above 30 RPS, the disturbance is driven by higher harmonics of the reaction wheel. These begin to excite the modes around 180 Hz. This is beyond the bandwidth of the optical control, so that there is no difference between the open and closed loop. Although these are not the actual wheels to be used on SIM, note that with the HST wheels the requirement is not met for some wheel speeds. Figure 18 shows that the Star WFT #1 metric never exceeds the requirements, which is consistent with the predictions made by the broadband analysis. Star OPD #2 results consistently show worse performance than #1 and 3 for both the broadband and narrowband analyses. Also the 180 Hz region appears to be critical, confirming broadband results, since the peak at 66 RPS is a result of the

2.82 wheel harmonic interacting with a 186 Hz structural mode. This will be analyzed in more depth in section 4.

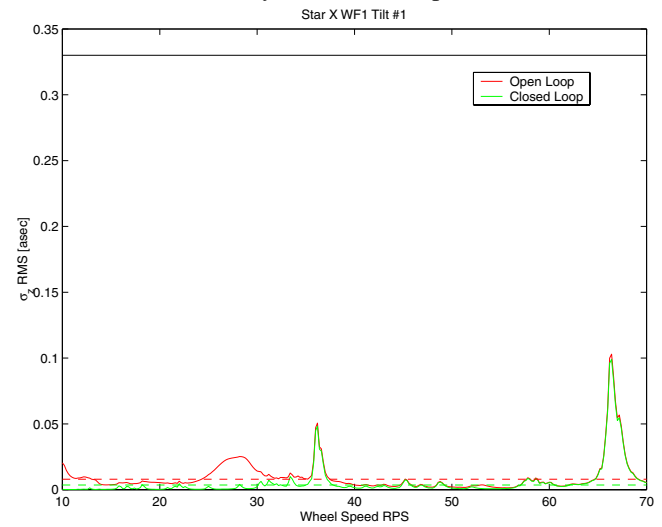


Figure 18 Narrowband disturbance analysis for Star WFT#1

A subsequent analysis by JPL revealed that the dynamic amplification in the 180 Hz region is due to a coupling between optics mount modes and isolator strut (bending) modes. The problem was resolved after the optical mount modes were significantly stiffened above 200 Hz. Table 2 summarizes and compares the broadband and narrowband disturbance analysis results. The broadband and narrowband-average results provide the “on-average” RMS of the performance metrics. The narrowband analysis maxima can be taken as a prediction of the “worst-case” RMS performance of the system. This can be relevant if a fringe tracker loses lock due to such a disturbance peak.

4. CRITICAL WHEEL SPEEDS AND MODES

Critical Wheel Speeds

Performance versus wheel speed curves as shown in Figures 17 and 18 were generated for all of the performance outputs. They were examined to determine which wheel speeds were

Table 2 Comparison of Broadband and Narrowband RWA disturbance analysis results

Performance	Open Loop			Closed Loop			Requirement
	broadband σ_z	narrowband average σ_z	narrowband maximum σ_z	broadband σ_z	narrowband average σ_z	narrowband maximum σ_z	
Star Opd #1 [nm]	45.6	28.23	171.56	8.26	3.17	27.81	10
Star Opd #2 [nm]	60.8	34.92	295.19	40.7	11.76	283.64	10
Star Opd #3 [nm]	46.8	28.87	186.07	7.51	3.23	38.19	10
Int. Met. Opd #1 [nm]	nc	49.53	342.31	16.69	6.43	57.10	20
Int. Met. Opd #2 [nm]	nc	65.91	588.31	80.85	23.36	565.29	20
Int. Met. Opd #3 [nm]	nc	52.17	371.23	14.89	6.41	76.09	20
Star WFT #1 [asec]	0.0154	0.0080	0.062	0.0131	0.004	0.060	0.21
Star WFT #2 [asec]	0.0159	0.0082	0.073	0.0138	0.004	0.070	0.21
Star WFT #3 [asec]	0.0184	0.0082	0.089	0.0166	0.005	0.085	0.21

critical for the optical performances. It was found that there are ranges of critical speeds: 30 to 32 RPS, 36 RPS, 50 to 60 RPS, and 66 RPS, where the latter was consistently the worst case (closed loop). Since it is undesirable to restrict the wheel speed ranges from an operational standpoint, we attempted to understand the reasons for the sharp peaks in the RPS vs. performance curves. Two examples are given below. Using the state-space models, continuous PSD plots can be generated by computing transfer functions. The cumulative RMS is the integral under these PSD plots. These plots can show which frequencies contribute most to the total RMS. Note that only one wheel speed at a time can be examined in this fashion.

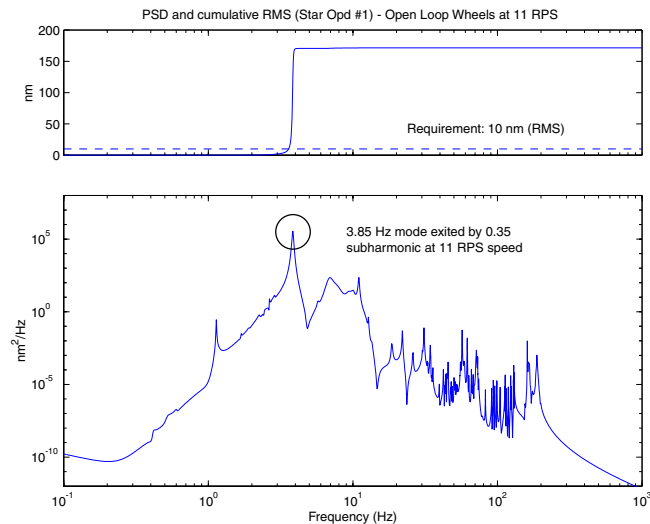


Figure 19 Narrowband wheel disturbance analysis (Star OPD#1), open optics loops, wheels at 11 RPS

Those speeds corresponding to the peaks were selected, such as 11 RPS in the open loop case (see Figure 19). Note that the fundamental wheel harmonic does not play a role in this or any of the narrowband performance PSD's analyzed.

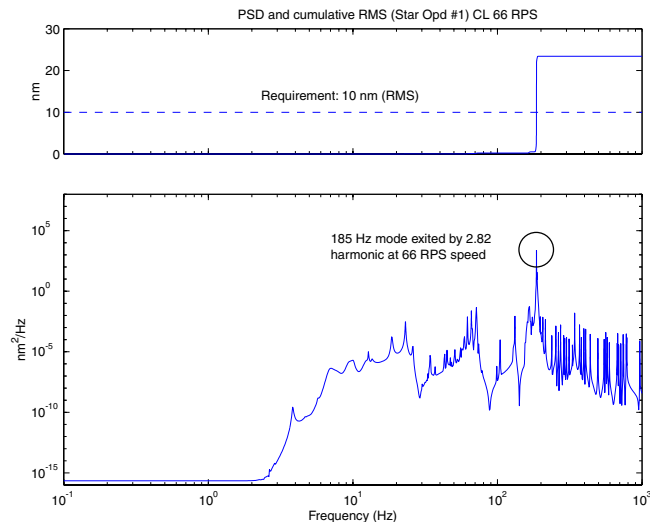


Figure 20 Narrowband HST-wheel disturbance analysis (Star OPD#1), 66 RPS, optics loops closed

This is most likely related to the fact that the HST wheels were very carefully balanced to reduce the effects of flywheel imbalances [9]. This is confirmed by consulting the tonal magnitudes in Figure 14. The main contribution at 11 RPS (open loop) comes from the 0.35 sub-harmonic exciting a 3.85 Hz mode as seen in Figure 19. In Figure 20, the closed loop performance Starlight OPD #1 at 66 RPS is driven by the 2.82 harmonic exciting a mode at 185 Hz.

Critical Modes Determination

At this point it is desirable to find the critical modes of SIM, i.e. the dynamics that appear to be major contributors to the RMS and RSS metrics discussed here. These modes can point to physical parameters and control parameters to modify for performance improvements. The critical modes determination will be based on the broadband disturbance model. There are several methods for finding the critical modes of the system. The first method plots and finds the largest modal gains (used by JPL), see Figure 21. Then the largest modal gains can be extracted as shown in the lower subplot of Figure 21. For the OPD metrics (combined) the critical modes appear to be clustered in the 6.85-7.85 Hz, 163.2-165.5 Hz and 184-187 Hz regions. A disadvantage of this method is that it does not take into account frequency weighting by the disturbance. This could explain why, the 6-7 Hz modes have high modal gains but do not contribute significantly to the closed loop performance as predicted by the broadband analysis (see Figure 11).

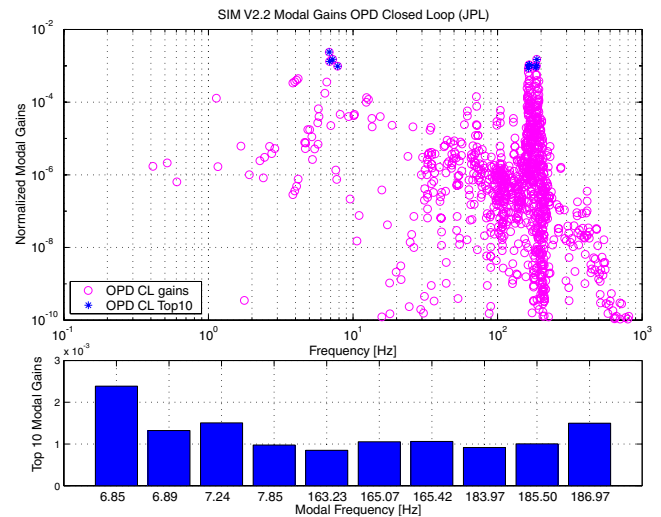


Figure 21 Modal gain plot for OPD's and top 10 modes

A second method developed by Gutierrez [7] is to find the “steps” in the cumulative RMS curve and correlate them with modal frequencies. Figure 22 shows from top to bottom the cumulative RMS curve, performance PSD curve and input contributions for Star OPD #2. The analyst interactively selects steps in the cumulative RMS curve in order to identify the modes and their relative contribution to the total RMS [7]. A problem was found with this method. If the modal density is high it is difficult to subjectively

decide, where one mode starts and stops. Also if a mode is highly damped, the rise in RMS will not be a sharp step, but rather a gradual increase. Thus, since the method requires user interaction, it lacks repeatability and is not generally applicable to large order systems such as SIM.

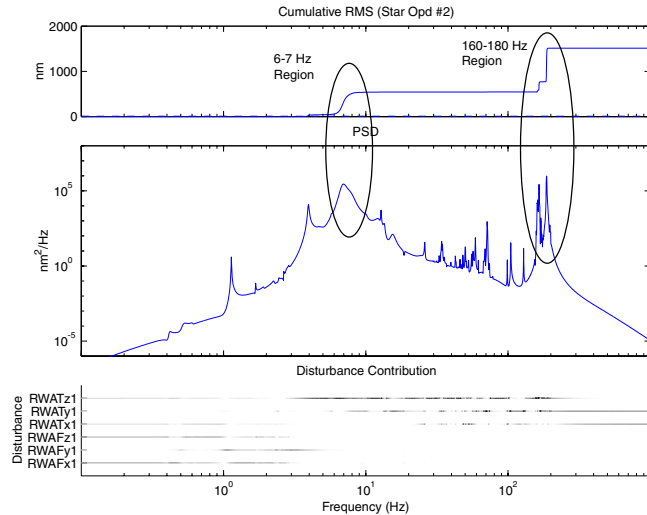


Figure 22 Cumulative RMS for critical mode determination (top subplot) for Star OPD #2. Middle plot shows Star OPD #2 power spectral density. Bottom plot shows relative contribution strength from six disturbance channels.

The third (bottom) subplot in Figure 22 shows the contribution of each of the six disturbance components as a function of frequency. The dark line for RWA Tz between 5 and 100 Hz suggests that it is the dominant disturbance component over this frequency range. A third method (Figures 23 and 24) uses a singular value decomposition (SVD) of the state covariance matrix Σ_q to determine the modal contributions to the total RMS via the solution of Lyapunov equations for each modal 2x2 block. This assumes that the overall state space system described in section 2 has been transformed into 2x2 modal block as follows:

$$\begin{bmatrix} -\zeta_n \omega_n & \omega_n \sqrt{1-\zeta_n^2} \\ -\omega_n \sqrt{1-\zeta_n^2} & -\zeta_n \omega_n \end{bmatrix} \quad (4.1)$$

Here ω_n and ζ_n are the n-th modal frequency and damping ratio respectively. The performance covariance matrix Σ_z (containing the individual performance variances from Table 1 on the diagonal) is decomposed as follows:

$$\Sigma_z = \text{diag} \{ \sigma_{z,i}^2 \} = C_z \underbrace{U \sqrt{S} \sqrt{S^T} U^T}_{\Sigma_q} C_z^T \quad (4.2)$$

where Σ_q is the state covariance matrix, S is the matrix of singular values and U is the unitary matrix resulting from the SVD. This allows decomposing the variance contributions to the i-th performance from each mode as shown in equation (4.3). The j-th column of the right matrix in (4.3) is the

variance contribution from the j-th mode. Note that mixed terms have to be broken up in a weighted fashion according to the singular values of each mode.

$$\Sigma_{z,i} = I_{1,xn} \begin{bmatrix} \vdots & \vdots & \vdots \\ C_{z,i,1} u_1 \sqrt{s_1} & \cdots & C_{z,i,n} u_n \sqrt{s_n} \\ \vdots & \vdots & \vdots \end{bmatrix}^2 \quad (4.3)$$

Plotting the modal variance contributions for Star OPD #2 results in the bar chart of Figure 23. The x-axis shows the modal frequencies and the y-axis shows the percent contribution to the performance RMS.

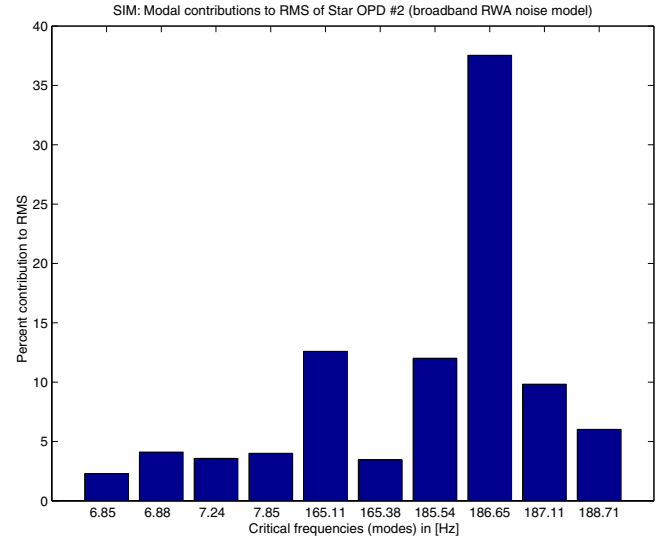


Figure 23 Critical modes for SIM Star OPD #2 using singular value decomposition of Σ_q (third method)

The correctness of the method can be confirmed by reconstructing the cumulative RMS curve (normalized according to [7]) from equation (4.3). Figure 24 overplots the reconstructed RMS curve and the cumulative RMS curve from the PSD analysis, they are seen to coincide well.

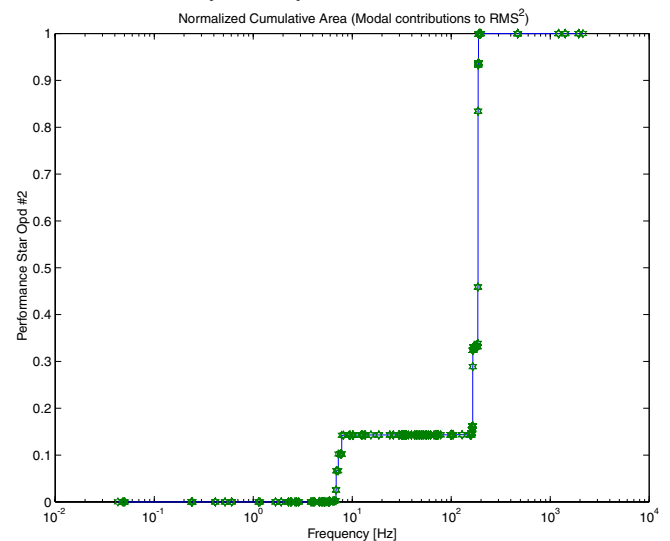


Figure 24 Reconstructed cumulative RMS curve (third method) and cumulative RMS from PSD analysis for Star OPD #2 metric

5. SENSITIVITY AND ISOPERFORMANCE

Modal Sensitivity Analysis

The theory of modal sensitivity analysis is developed by Gutierrez in reference [7]. Essentially a Lagrange multiplier approach is used to obtain analytical sensitivities of the performance RMS and RSS values with respect to modal parameters. Figure 25 shows the results for the modal parameter sensitivity analysis for Star OPD #2 (closed loop) in the frequency region from 170-190 Hz. The modal parameters are the modal frequency, the modal damping ratio and the modal mass. The x-axis of the plot corresponds to the normalized sensitivity. A value of +1 for example indicates that a positive change of 1% in the modal parameter will result in approximately a 1% increase in the RMS. The largest sensitivities are found for the modes in the 180-190 Hz region. The phasing/OPD performance is very sensitive to these modes. The largest sensitivities were found for the modes at 185.5, 186.7 and 187.1 Hz with respect to the modal frequencies.

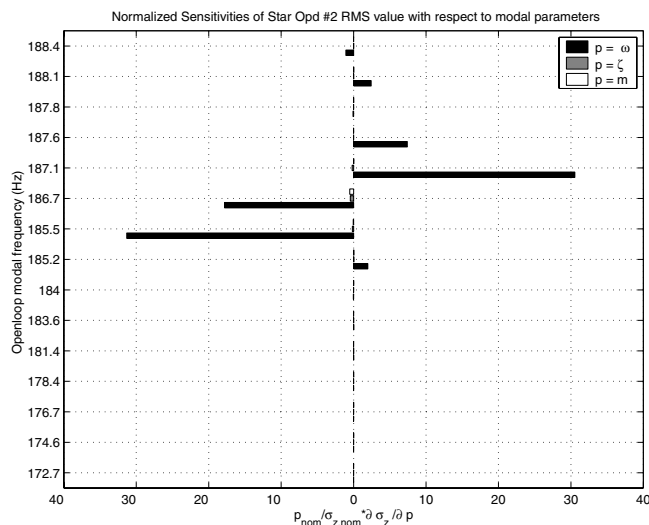


Figure 25 Sample modal sensitivity analysis results for SIM (Star OPD #2) metric, optics loops closed

Finite Difference Verification

We conducted a finite difference analysis in order to confirm or reject this result. The finite difference approximation of the normalized sensitivity is as follows:

$$\frac{\partial \sigma_z}{\partial p} \cdot \frac{p_{nom}}{\sigma_{z,nom}} \cong \frac{\Delta \sigma_z}{\Delta p} \cdot \frac{p_{nom}}{\sigma_{z,nom}} \quad (5.1)$$

Here $\partial \sigma_z / \partial p$ is the partial derivative of the performance RMS with respect to a system parameter, p_{nom} is the nominal parameter value and $\sigma_{z,nom}$ is the nominal RMS value. The results of this finite difference analysis are shown in Table 3 for damping and frequency. The finite difference approximation uses a 1% perturbation size on the modal

parameters. The comparison between the analytical sensitivities and the finite difference approximation corroborate the modal sensitivity analysis results. A possible explanation for these large modal sensitivities with respect to frequency is related to a modal density consideration. Several regions of high modal density can be observed for SIM. One of these regions is the 160-190 Hz region, which has been confirmed as being problematic for SIM.

Table 3 Finite Difference Results for Star OPD #2

Sensitivities with respect to damping ζ :		
Mode #	Analytical	Finite Difference
148 (185.2 Hz)	3.095e-002	3.226e-002
149 (185.5 Hz)	-1.773e-001	-1.742e-001
150 (186.7 Hz)	-4.497e-001	-4.453e-001
151 (187.1 Hz)	-2.086e-001	-2.057e-001
152 (187.6 Hz)	-2.966e-003	-1.456e-003
Sensitivities with respect to frequency ω :		
Mode #	Analytical	Finite Difference
148 (185.2 Hz)	1.97e+000	1.26e+001
149 (185.5 Hz)	-3.13e+001	-2.73e+001
150 (186.7 Hz)	-1.78e+001	-3.11e+001
151 (187.1 Hz)	3.05e+001	-2.01e+000
152 (187.6 Hz)	7.42e+000	2.93e+000

Isoperformance Analysis

An isoperformance analysis involves holding the opto-mechanical performance fixed (corresponding to an equality constraint in an optimization problem) and trading variable system parameters with respect to each other. We have seen in section 3 that the pointing metrics (WFT) easily meet performance, while the OPD phasing requirements are more challenging to meet. An interesting tradeoff is between a reduction in disturbance magnitude (reducing imperfections in the reaction wheels) and higher bandwidth optical control. The isoperformance trade considered here involves the gain factor on the RWA state space overbound K_{rwa} from equation (3.1) and the optical control bandwidth (corner frequency) $f_o = \omega_o / 2\pi$, which was introduced in equation (2.4). The performance we are constraining is Star OPD #1. We are interested in two performance RMS levels: 3 and 6 nm. Figure 26 summarizes the isoperformance problem setup.

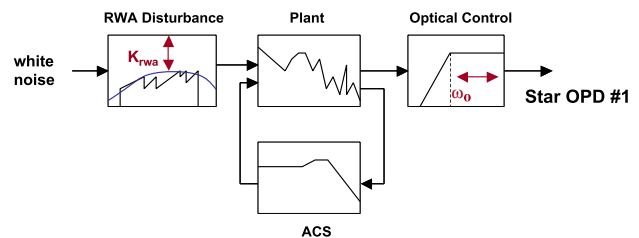


Figure 26 SIM isoperformance problem setup

The key equations that underlie the isoperformance method

are as follows:

$$\sigma_z(p) = \sigma_z(p_k) + \underbrace{\nabla \sigma_z^T \Big|_{p_k}}_{\text{first order term}} \Delta p + \underbrace{\frac{1}{2} \Delta p^T H \Big|_{p_k}}_{\text{second order term}} \Delta p + \text{HOT} \quad (5.2)$$

Here p represents the vector of variable parameters and the performance (vector) functional $\sigma_z(p)$ is expanded in a Taylor series. A steepest gradient search is used to intersect the performance contour of interest starting from an initial guess. Then the step direction along the contour (tangent following) is determined from the nullspace of the gradient vector $\nabla \sigma_z$ (Jacobian in the multivariable case):

$$\nabla \sigma_z^T \Big|_{p_k} \Delta p \equiv 0 \quad (5.3)$$

The step size along the contour is determined by inverting the Hessian matrix H in (5.2). Further details on the isoperformance algorithm are available from the authors [10]. Figure 27 shows the parameter-bounding box (red), which is given by the upper and lower bounds on the free parameters K_{rwa} and f_o . The two isoperformance curves are given in blue (6 nm) and green (3 nm). As expected we can improve the nominal performance for Star OPD #1, computed as 8.26 nm (Table 2) with $K_{rwa}=1$ and $f_o=100$ Hz, by increasing the control bandwidth or by reducing the RWA disturbance magnitude. Two distinct solutions **A** (low wheel disturbance – nominal control) and solution **B** (nominal wheel disturbance – aggressive control) are shown in Figure 27.

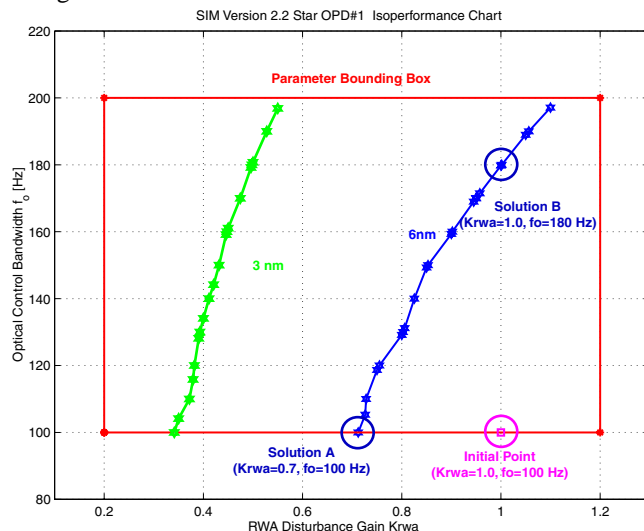


Figure 27 Isoperformance analysis results for SIM

It appears intuitive that a reduction in wheel disturbance magnitudes (across all harmonics) down to 70% of the experimentally determined HST-wheel levels should be easier to achieve than an increase of the optical phasing control loop bandwidth from 100 to 180 Hz. This conjecture should be confirmed by more in-depth analysis in the future.

From the slope of the isoperformance contours it appears that Star OPD #2 is more sensitive to changes in RWA disturbance magnitudes than changes in control bandwidth.

6. CONCLUSIONS & RECOMMENDATIONS

Conclusions

This section summarizes some of the observations and issues that were detected during the research on the integrated SIM model (version 2.2). Some issues have surfaced with this new model that have not been seen in previous analyses such as a mix of highly resonant individual structural and damped ‘clusters’ of modes. The very large number of states >2000 required careful model conditioning and reduction.

The fundamental harmonic of wheel disturbance is not a performance driver in the narrowband analysis case for the Hubble-type wheels. The region from 160 to 190 Hz is critical to the closed loop performance of SIM. Unfortunately this region is outside of the optical control bandwidth (100 Hz). A relative reduction in wheel disturbance magnitude appears more beneficial for SIM than extending the optical control bandwidth. The narrowband wheel speed analysis is recommended for finding the maximum expected occurrences of OPD and WFT (“worst case analysis”), whereas the broadband analysis provides a measure of the “on average” dynamic performance. Both analyses are complementary to each other.

Recommendations

Future work should include leveraging the isoperformance analysis for dynamics error budgeting. This would involve including other disturbance sources than the RWA in the integrated model such as attitude determination noise, microdynamics etc. The predictive accuracy of the FEM can be within a few % for the first dozen flexible modes, but then degrades for higher frequency modes. It appears, however, that the dynamics above 100 Hz, outside the bandwidth of optical control, are the dominant contributor to the residual OPD and WFT jitter. This is especially true when unexpected modal interaction between higher order structural, isolator and optical mount modes occur. A concurrent modeling and test strategy should be devised to address the issue of these uncertain dynamics above 100 Hz for SIM, once optics and attitude control loops are closed.

ACKNOWLEDGMENTS

Part of the work described in this paper was conducted at the Massachusetts Institute of Technology under contract from the Jet Propulsion Laboratory, California Institute of Technology (Contract Number 961-123), with Robert Grogan as contract monitor. Part of the work described in this paper was carried out at the Jet Propulsion Laboratory, California Institute of Technology, under contract with the National Aeronautics and Space Administration.

LIST OF ACRONYMS

ACS	Attitude Control System
DOCS	Dynamics Optics Controls Structures
HPF	High Pass Filter
HST	Hubble Space Telescope
LPF	Low Pass Filter
LTI	Linear Time Invariant
OPD	Optical Pathlength Difference
PSD	Power Spectral Density
RMS	Root-Mean-Square
RPS	Revolutions per second
RSS	Root-Sum-Square
RWA	Reaction Wheel Assembly
SIM	Space Interferometry Mission
WFT	Wavefront Tilt
nm	nanometers
asec	arcsecond

REFERENCES

- [1] Stephen C. Unwin, Rudolf Danner, Slava G. Turyshev and Michael Shao, "Science with the Space Interferometry Mission", SIM Memorandum, Jet Propulsion Laboratory, 1997. (Internal JPL document)
- [2] M. M. Colavita, M. Shao, and M. D. Rayman, "Orbiting stellar interferometer for astrometry and imaging," *Applied Optics*, vol. 32, no. 10, pp. 1789-1797, 1993.
- [3] Basdogan, I., Grogan, R., Kissil, A., Sigrist, N., and Sievers, L., "Preliminary Optical Performance Analysis of the Space Interferometry Mission using an Integrated Modeling Methodology," Proceedings of the International Mechanical Engineering Congress & Exposition, October 2000.
- [4] Kemin Zhou, Jon C. Doyle and Keith Glover, "Robust and Optimal Control", Prentice Hall Publishers, Upper Saddle River, New Jersey, 1996
- [4] Moore, B., "Principal Component Analysis in Linear Systems: Controllability, Observability and Model Reduction", IEEE Transactions on Automatic Control, 26-1, February 1981
- [5] Laub, A., "Computation of Balancing Transformations", Proceedings of JACC, Volume 1, paper FA8-E, 1980
- [6] Mallory, G., "Development and Experimental Validation of Controller Tuning Technique for Spaceborne Telescopes", Ph.D. thesis, Department of Aeronautics and Astronautics, M.I.T., April 2000
- [7] Gutierrez, H., "Performance Assessment and Enhancement of Precision Controlled Structures During Conceptual Design", Ph.D. thesis, Department of Aeronautics and Astronautics, Massachusetts Institute of Technology, February 1999
- [8] Masterson, R., "Development and Validation of Empirical and Analytical Reaction Wheel Disturbance Models", S.M. thesis, Massachusetts Institute of

Technology, June 1999

- [9] Hasha, M.D., "Reaction Wheel Mechanical Noise variations", Engineering Memorandum, EM No. SSS-218, Space Telescope Program, 30 June 1986
- [10] de Weck, O.L., "Introduction to Isoperformance Analysis for Precision Opto-Mechanical Space Systems – Application to Bivariate Problems", Research Memorandum, Massachusetts Institute of Technology, May 2000 (MIT internal document)
- [11] Uebelhart, S.A., "Model Conditioning for Large Order State Space Representations of Space Telescopes", S.M. thesis, Massachusetts Institute of Technology, Jan 2001.

AUTHOR BIOGRAPHIES

David W. Miller is an Associate Professor at the M.I.T. Department of Aeronautics and Astronautics. His research interests include controls/structure interaction, distributed satellite systems, space based astronomy and modularity in space systems design. He has published numerous conference and journal articles on space systems and has been involved in the MACE (Middeck Active Control Experiment) Space Shuttle and other flight experiments.

Olivier de Weck is a Ph.D. candidate at the Space Systems Laboratory (SSL) at M.I.T. and specializes in integrated modeling and dynamics of spaceborne observatories for visual and IR astronomy. He has a background in non-linear FEM simulation, industrial process management and systems engineering. Previously he was a liaison engineer and engineering program manager on the Swiss F/A-18 aircraft program at McDonnell Douglas (now Boeing Company) in St. Louis, Missouri.



Scott A. Uebelhart (SB, MIT, 1998) is a Masters Student in the MIT Space Systems Laboratory. His Masters thesis concerns model reduction and quality management for large space structures. He will begin Ph.D. studies in January 2002, after spending a year working for Daimler Chrysler outside of Munich, Germany. His research interests include structures/controls interactions in flexible space structures.

Robert Grogan is a Senior Member of the Engineering Staff at the Jet Propulsion Laboratory. Previously he was a Staff Engineer at AlliedSignal Aerospace and he holds one patent. He received a B.S. degree from Penn State in 1992 and a M.S. degree from Virginia Tech in 1994. His work has been in the areas of interferometry, multi-disciplinary modeling, dynamics, control, neural networks, and systems engineering.

Ipek Basdogan, Ph.D., is a member of the technical staff in Mechanical Engineering Section at the Jet Propulsion Laboratory. She received her Ph.D. in mechanical engineering from University of Illinois at Chicago in 1997. Before joining JPL, she worked as a Laboratory Graduate at Argonne National Laboratory-Advanced Photon Source. Her research interests include modeling of opto-mechanical and electro-mechanical systems, dynamics and structural analysis, testing and experimental analysis.



APPENDIX

DOCS FRAMEWORK DESCRIPTION

The DOCS (Dynamics-Optics-Controls-Structures) framework developed for this research is a powerful toolset for the modeling and analysis of precision opto-mechanical space systems. Within the MATLAB™ environment a model of the spacecraft can be created, which simulates the dynamic behavior of the structure, the optical train, the control systems and the expected disturbance sources in an integrated fashion (see Figure below).

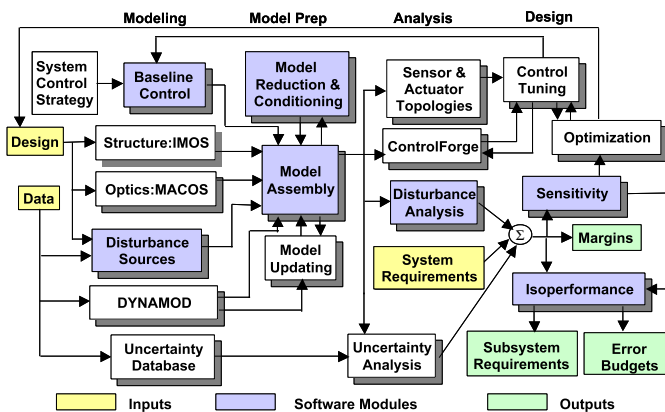


Figure A DOCS framework block diagram

The existing toolboxes are compatible with IMOS (Integrated Modeling of Optical Systems), a JPL developed MATLAB-based opto-structural modeling toolbox, MSC/NASTRAN, a commercial FEM solver, as well as DynaMod and ControlForge, two measurement model and control synthesis packages developed by Midé Technology Corporation (<http://www.mide.com>). Once an initial model has been created and numerically conditioned, the root-mean-square (RMS) values of scientific and opto-mechanical performance metrics of the system (e.g. pathlength difference, pointing jitter, fringe visibility, null depth) can be predicted.

The exact sensitivities of the RMS with respect to modal or physical design parameters can be computed. These sensitivities are essential for conducting gradient-based optimization, redesign or uncertainty analyses. The goal of the uncertainty analysis is to associate error bars with the predicted RMS values, which are based on an uncertainty database resulting from past ground and flight experience. The actuator-sensor topology of the system can be analyzed numerically to ensure that the control system uses the actuator-sensor pairs that will ensure maximum disturbance rejection or tracking performance.

Once a design has been found that meets all requirements with sufficient margins, an isoperformance analysis can be conducted. Treating the performance as a constraint the expected error sources (error budgeting) or key design parameters (subsystems requirements definition) can be traded with respect to each other.

If hardware exists, the experimental transfer functions can be used to update the structural, avionics and uncertainty models throughout the life of the program to achieve a convergent design that will achieve mission success. Preliminary versions of the framework have been successfully applied to conceptual designs of SIM, NGST, TPF and Nexus.